

*ICTP-IAEA Workshop on “The training in basic radiation materials science and its applications to radiation effects studies and development of advanced radiation-resistant materials”  
Trieste, 10 – 21 November 2008*

---

# Mechanisms of RPV embrittlement

V.A. Pechenkin

SSC RF Institute of Physics & Power Engineering,

Obninsk, Russia

# Outline

- Irradiation embrittlement
- Embrittlement mechanisms
- Irradiation and metallurgical variables
- Models of embrittlement induced by hardening
- Embrittlement enhancement in VVER-440s at high neutron fluences
- Contribution of intergranular (nonhardening) embrittlement
- Modeling of embrittlement at high neutron fluences

# Introduction

Light water reactors generate a large majority of the world's nuclear energy. Achieving reasonable thermodynamic efficiency requires a heavy-section steel reactor pressure vessel (RPV) to safely contain coolant water at temperatures around 290°C at pressures ranging from 7 MPa in boiling water reactors (BWR) to 14 MPa in pressurized water reactors (PWR).

Regulations require very low RPV failure probabilities both for normal operation and postulated accident events.

Neutron irradiation embrittlement could limit the service life of some of the reactor-pressure vessels in existing commercial nuclear-power plants.

# VESSELS

RPVs are massive welded structures, weighing up to 500 tonnes, standing 14 m high by 4.5 m in diameter with a wall thickness up to 20 cm or more.

Vessels operate at temperatures ( $T_{\text{irr}}$ ) of about  $290 \pm 30^\circ\text{C}$  and are exposed to a spectrum of neutron energies ranging from less than one to several million electron volts (MeV).

High-energy neutrons are the dominant source of embrittlement. The neutron flux ( $\Phi$ ) is defined as the number of neutrons crossing a unit area per unit time (neutrons/m<sup>2</sup> -s) and the neutron fluence ( $\Phi t$ ) is the flux integrated over time (neutrons/m<sup>2</sup>). A standard unit of neutron exposure is the  $\Phi t$  greater than 1 MeV ( $\Phi t > 1$ ). The end-of-life  $\Phi t > 1$  for U.S. PWRs is about  $1\text{--}3 \times 10^{23}$  n/m<sup>2</sup>, and about an order of magnitude lower in BWRs.

For more details on neutron spectra and radiation damage in RPVs – see Pechenkin4

# Irradiation embrittlement

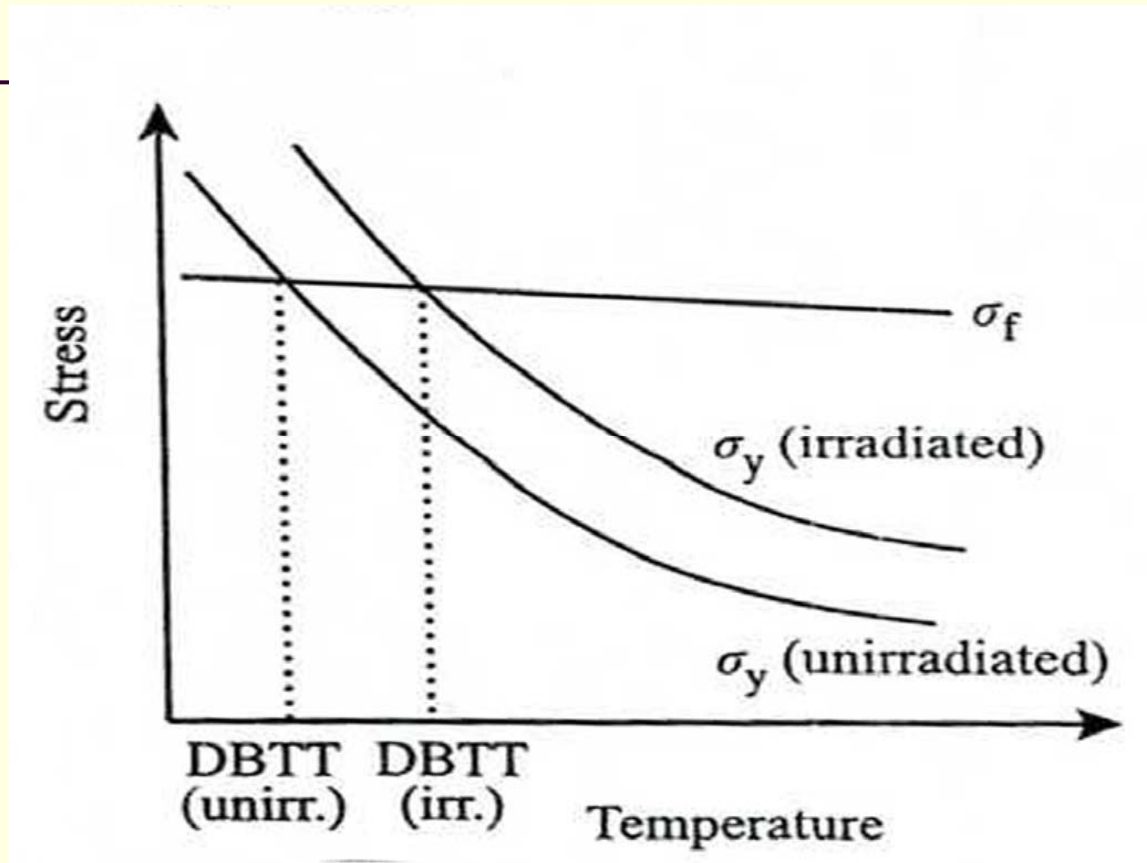
The ductile-to-brittle transition temperature (DBTT) is defined by the condition that yield stress  $\sigma_y$  equals fracture stress  $\sigma_F$ .

Irradiation embrittlement is usually characterized by the increase in a DBTT ( $\Delta T$ ) that marks the transition between low toughness brittle (cleavage) and high toughness ductile fracture regimes.

Transition temperature shifts have exceeded 200°C in some cases. Hence, embrittlement must be considered in RPV integrity assessments and, if severe, may require either premature plant closure or vessel annealing.

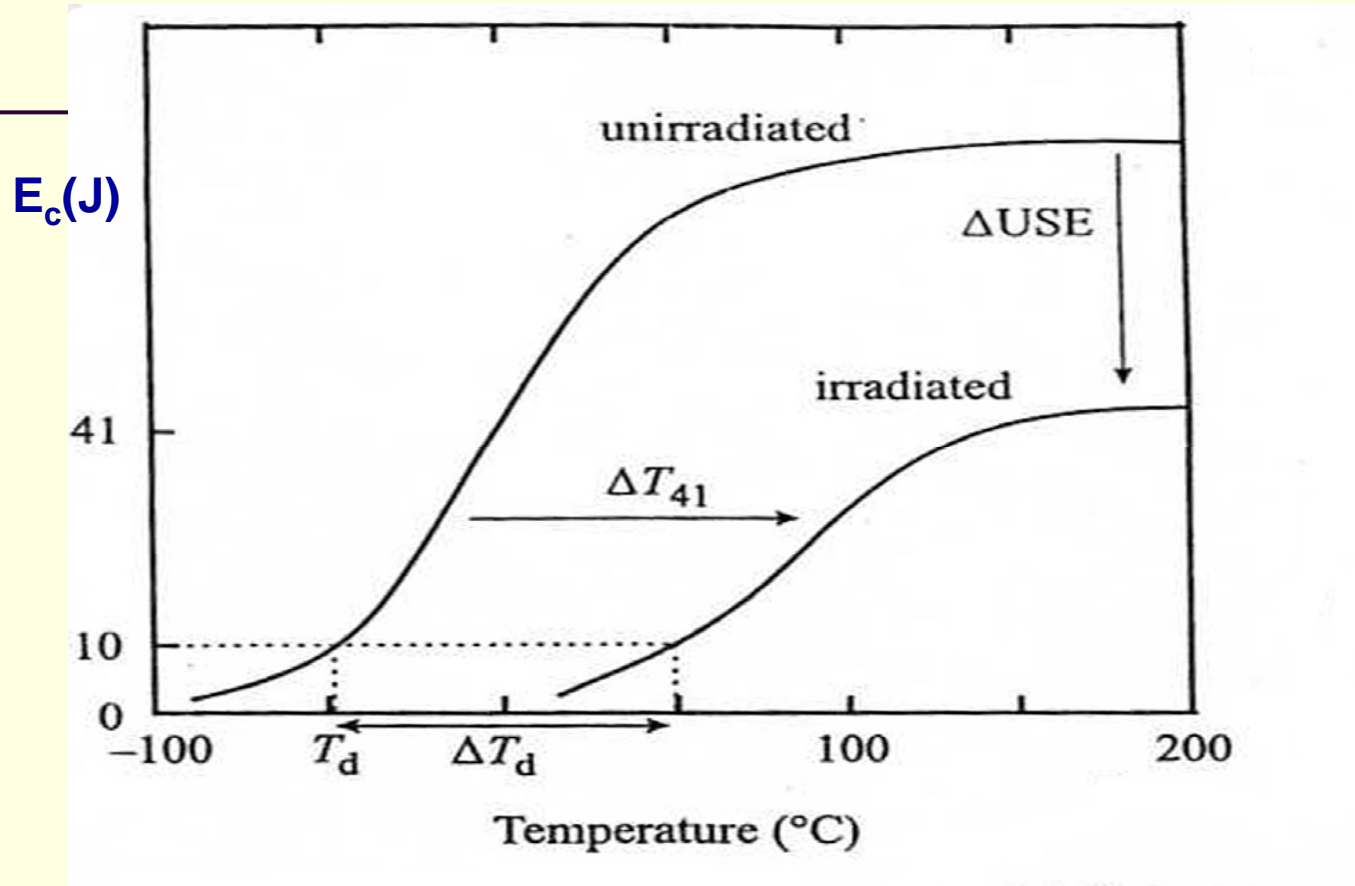
The primary cause of embrittlement in RPV steels is **irradiation hardening** produced by nanometer features that develop as a consequence of irradiation.

# Hardening-Induced DBTT Shift



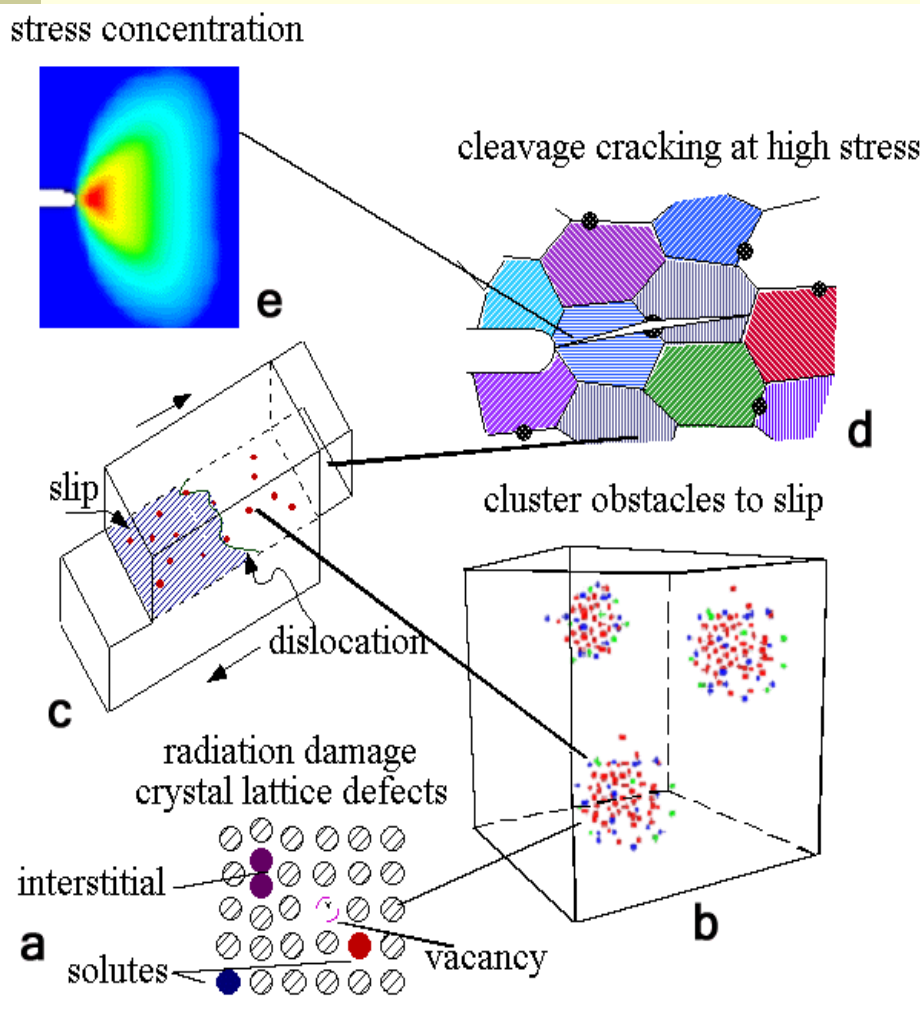
Usually an empirical relation between  $\Delta\sigma_y$  and  $\Delta T$  is observed:  
$$\Delta T \approx [0.6 \pm 0.2^\circ\text{C}/\text{MPa}] \Delta\sigma_y$$

# Charpy tests



Small  $10 \times 10 \times 55$  mm Charpy-V-notch (CVN) impact specimens are typically used in surveillance programs. The Charpy impact energy - temperature curve is used to determine a DBTT ( $T_t$ ), indexed at an absorbed energy of 41 Joules. Neutron irradiation elevates  $T_t$  (induces  $\Delta T_t$ ) and decreases the CVN upper-shelf energy

# Embrittlement mechanisms



- The primary mechanism of embrittlement is the hardening produced by nanometer features. The key embrittlement processes include:
- Generation of lattice defects in displacement cascades by high-energy recoil atoms from neutron scattering and reactions. The primary defects are in the form of single and small clusters of vacancies and self-interstitials ([Figure 1a](#)).
- Diffusion of primary defects also leading to enhanced solute diffusion and formation of nanoscale defect-solute cluster complexes, solute clusters, and distinct phases, primarily copper-rich precipitates (CRPs) ([Figure 1b](#)).
- Dislocation pinning and hardening by these nanofeatures ([Figure 1c](#)).
- *Hardening-induced  $\Delta T_t$  shifts* ([Figure 1d and e](#)).

(from Odette, 2001)

# Embrittlement mechanisms

The individual contribution of a particular nanofeature to hardening is given by

$$\Delta\sigma_j = \alpha_j M G b \sqrt{N_j d_j}$$

where  $M$  is the Taylor factor,  $G$  is the shear modulus,  $b$  is the Burgers vector, and  $N_j$  and  $d_j$  are the number density and diameter of the feature, respectively.

The  $\alpha_j(d_j)$  is a strength factor that depends on the details of the dislocation-obstacle interaction process, hence, the size and characteristics of the feature. For irradiation-induced nanofeatures in RPV steels, dislocation pinning is generally weak and  $\alpha_j(d_j)$  can be  $\ll 1$ .

A combination of experiments and computer simulations should be used to evaluate  $\alpha_j(d_j)$  and to establish superposition relations for typical irradiation-induced features.

## DBTT Shift

Commonly, the DBTT shifts are evaluated using regulatory equations based on a large collection of surveillance data from many plants.

The  $\Delta T$  is controlled by many variables. Recent, physically based, statistical fits to the U.S. surveillance database show that the  $\Delta T$  depends on  $T_{\text{irr}}$ ,  $\Phi$ ,  $\Phi t$ ; Cu, Ni, and P content, and product form (weld, plate, and forging).

Single-variable, test reactor studies show that  $\Delta T$  also depends on a number of other variables including Mn content and final heat-treatment conditions.

Predictive models must also account for strong synergistic interactions between variables, such as copper – nickel and others.

## Vessel steels

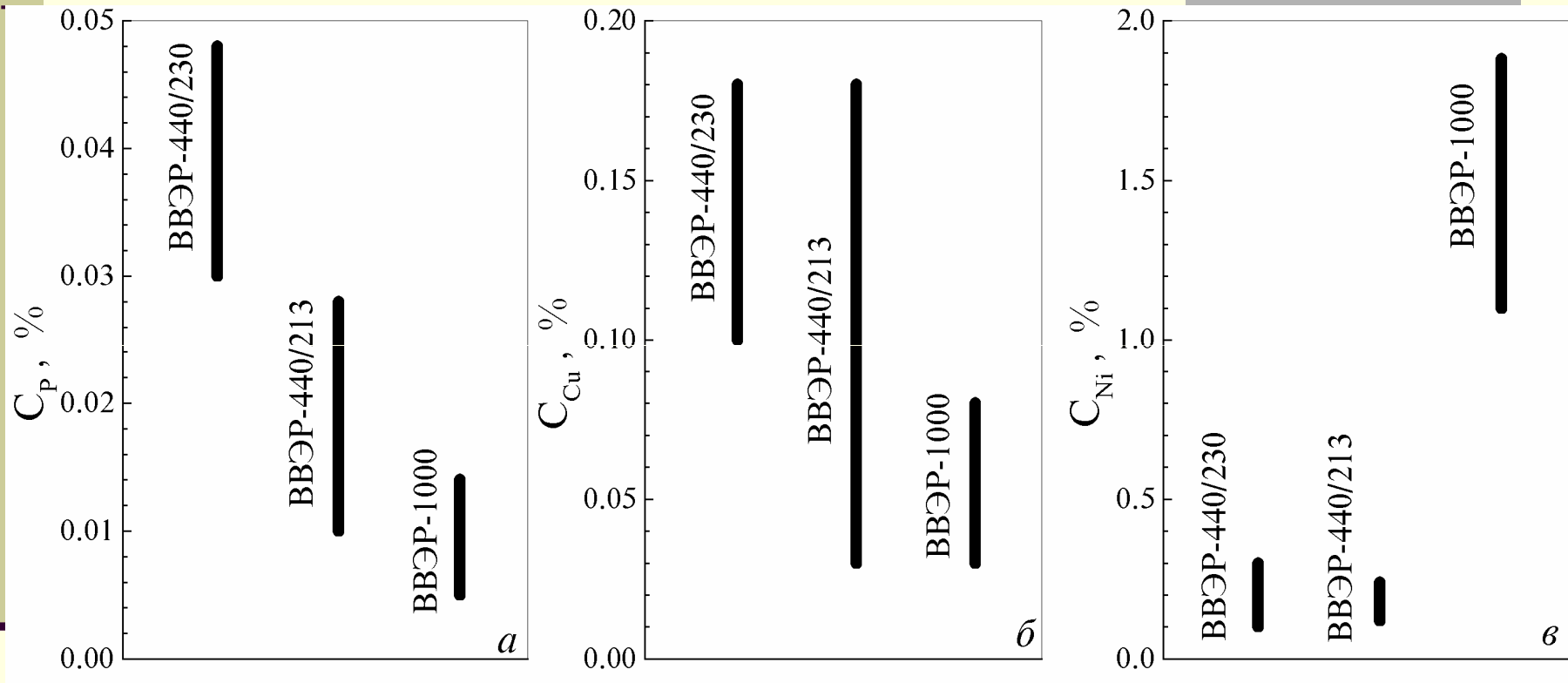
Typical RPV base metals in U.S. are A302B, A533B plates, or A508 forgings.

Typical compositions are C(0.05–0.2%), Mn(0.7–1.6%), Mo(0.4–0.6%), Ni(0.2– 1.4%), Si(0.2–0.6%), and Cr (0.05–0.5%).

Weld compositions differ from the base metal, and may vary significantly even within the same weld. Compositions and microstructures vary on both the macro- and micro-scales.

Along with nickel alloying additions, trace impurity copper and phosphorous increase embrittlement. Copper contents are quite high (up to 0.4%) in some early U.S. welds.

# Ni, P and Cu content in Russian VVER-440 and VVER-1000



High Ni content in RPV VVER-1000

# Irradiation Induced Nanostructures

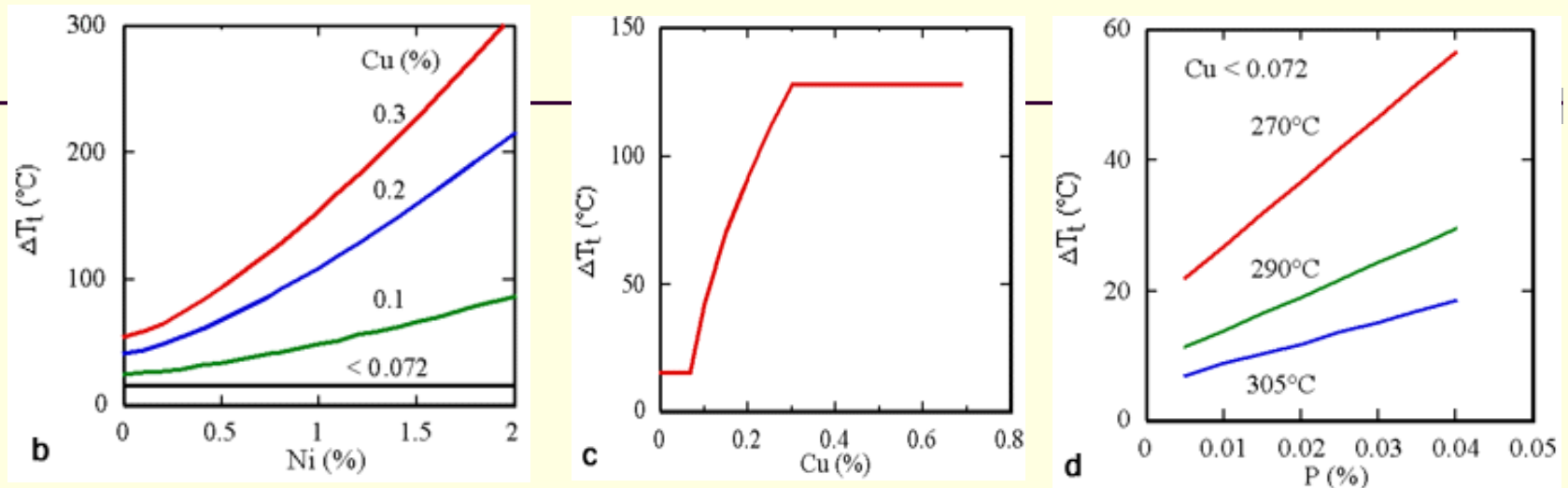
Key characterization methods include:

Small angle x-ray and neutron scattering,  
various types of electron microscopy,  
three-dimensional atom probe-field ion microscopy,  
positron annihilation spectroscopy.

While all of these tools have individual limitations, in combination they have provided considerable insight about the nanofeatures that can be divided into three broad categories:

- Copper rich or catalysed manganese-nickel rich precipitates (CRPs/MNPs).
- Unstable matrix defects (UMD) that form in cascades even in steels with low or no copper, but that anneal rapidly compared to typical low  $\Phi$  irradiation times.
- Stable matrix features (SMF) that persist or grow under irradiation even in steels with low or no copper

# Irradiation and metallurgical variables



Figures illustrate the dependence of  $\Delta T$  on some metallurgical variables. Unless otherwise indicated, the default variables are: welds,  $T_{\text{irr}} = 290^\circ\text{C}$ ,  $\Phi t = 10^{23} \text{ n/m}^2$ ,  $P = 0.01\%$ ,  $\text{Cu} = 0.3\%$ ,  $\text{Ni} = 0.8\%$  and  $\Phi = 5 \times 10^{14} \text{ n/m}^2$ .

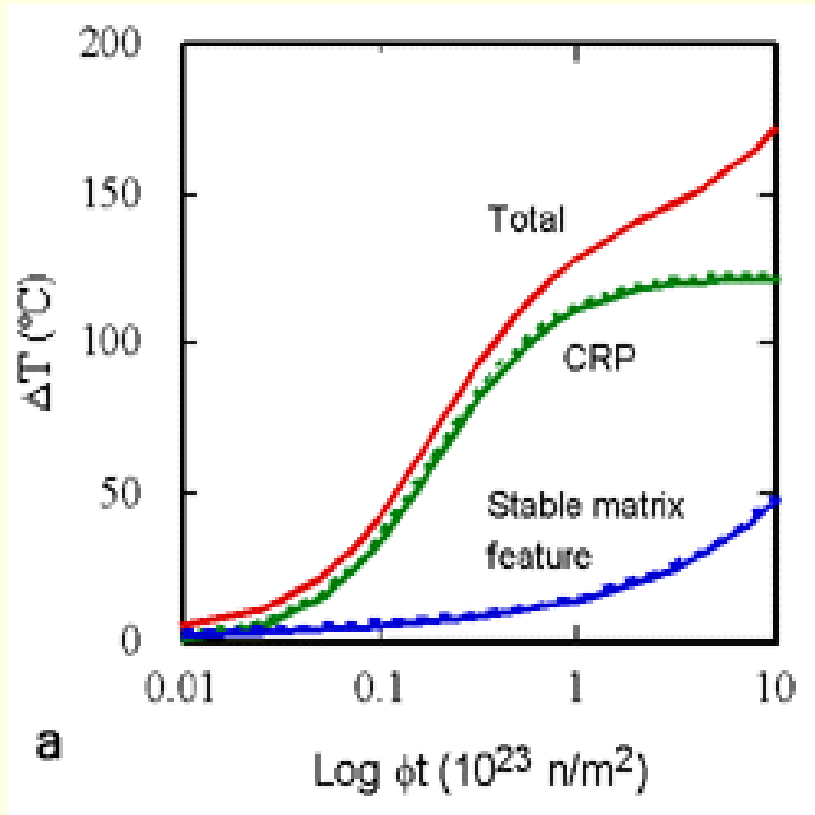
There is a very strong interaction between copper-nickel ([3b](#)).

The threshold and the effective maximum copper are about 0.07% and 0.3% ([3c](#)) due to the CRP nucleation and pre-precipitation limits, respectively.

The  $\Delta T$  due to the SMF increases with increasing P and decreasing  $T_{\text{irr}}$  ([3d](#)).

(from Odette, 2001)

# Two-feature model



A two-feature model (SMF and CRP) of the form

$$\Delta T = A f_{\text{smf}}(\text{Ti}, \Phi t, P) + B f_{\text{crp}}(\text{Cu}, \text{Ni}, \Phi, \Phi t),$$
 provides an excellent fit to the large (609  $\Delta T$  points) U.S. power reactor surveillance database, with a standard error of  $\pm 13^\circ\text{C}$ .

Both the coefficients for the SMF (A) and CRP (B) differ between welds, plates, and forgings.

The  $\Delta T$  due to the SMF increases roughly with the square root of  $\Phi t$  (from Odette, 2001)

# Account of intragranular segregation

For VVER-440 welds and PWR surveillance data analysis the evolution of the embrittlement in terms of  $DBTT_{shift}$  (shift in ductile to brittle transition temperature) is modelled as follows (Debarberis):

$$DBTT_{shift} = MD + CuPr + OPrSg$$

Where:

MD = Matrix Damage contribution

CuPr = Cu Lead Precipitations contribution

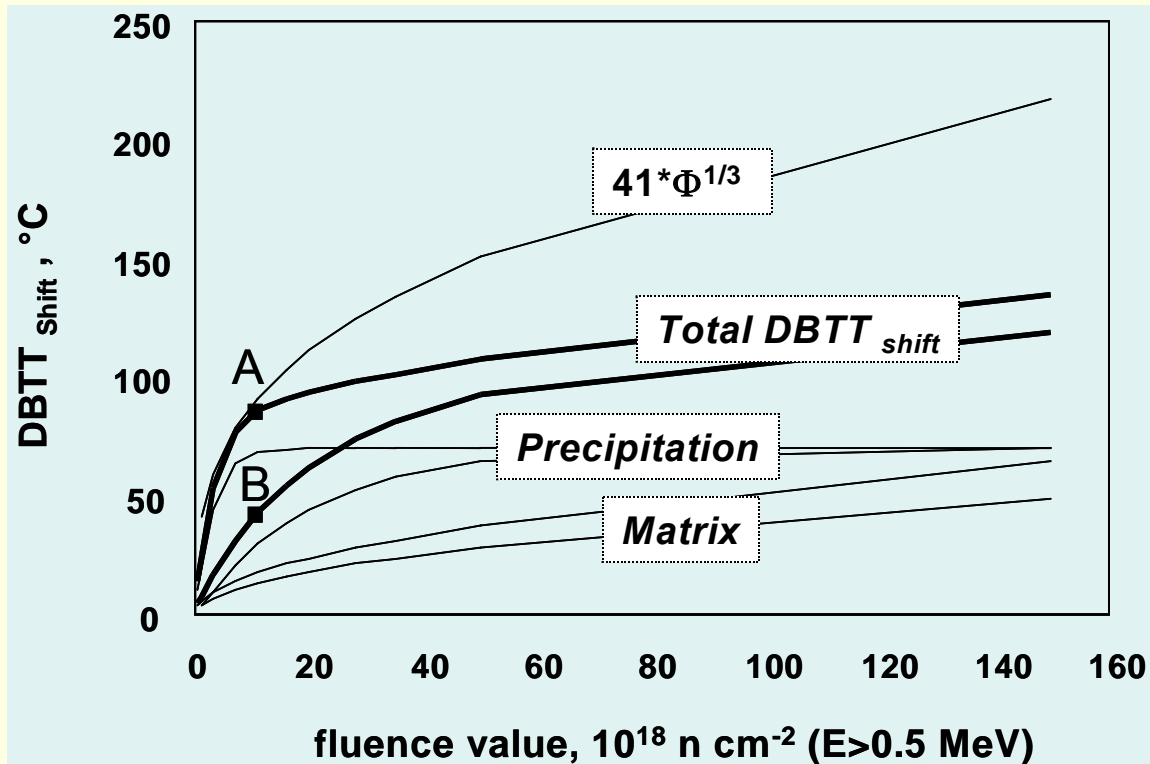
OPrSg = Other co-precipitations and intra-grain segregations

Based on the above mentioned partial effects, the total effect in term of transition temperature shift is detailed as follows:

$$DBTT_{shift} = a * \Phi^{0.5} + b * \left[ 1 - e\left(-\Phi / \Phi_{sat}\right) \right] + c / 2 * \left[ 1 + Tangh\left(\frac{\Phi - \Phi_{start}}{d}\right) \right]$$

**c is parameter function of P content**

# Account of intragranular segregation



Long-term damage prediction interpretation

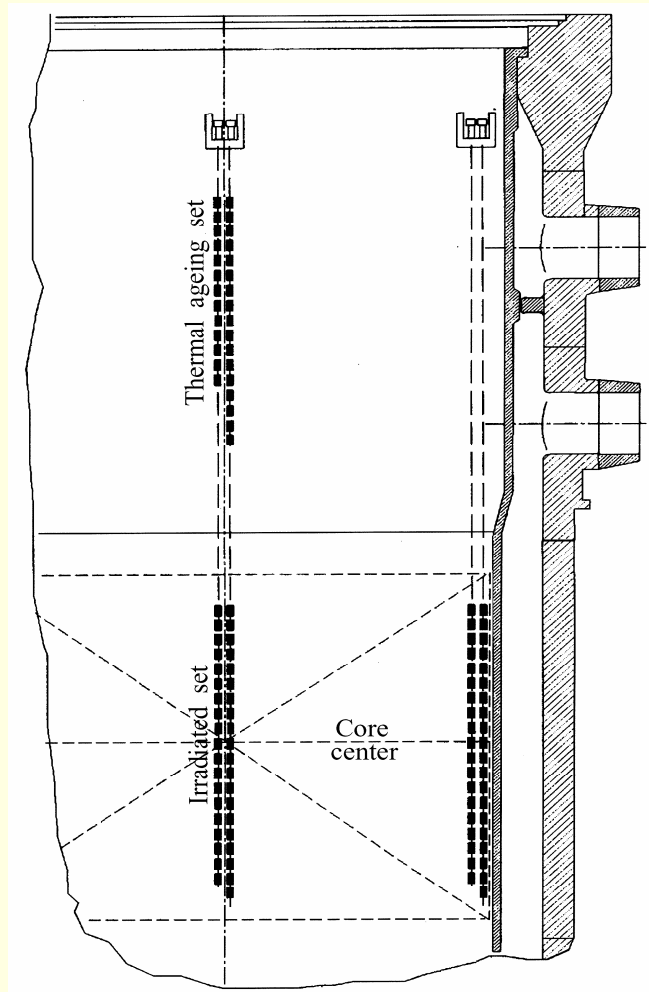
# Embrittlement enhancement in VVER-440s at high neutron fluences

Now it is considered, that hardening of the matrix is the basic mechanism of the reactor pressure vessel steel (RPVS) embrittlement in PWRs and VVER-440s at moderate doses (usually, at neutron fluences below  $\sim 10^{20}$  n/cm<sup>2</sup> ( $E > 0.5$  MeV)).

Even at these doses a considerable portion of intergranular fracture stipulated by grain boundary phosphorus segregation is observed on fracture surfaces.

*From the data on surveillance specimens for several units of VVER-440 an irradiation embrittlement enhancement has been observed at neutron fluences above  $(2-3) \times 10^{20}$  n/cm<sup>2</sup> ( $E > 0.5$  MeV) with a significant deviation from the standard guide and significant increase of intergranular (nonhardening) embrittlement .*

# Location scheme of the surveillance chains in WWER-440/213 pressure vessel



Surveillance chains are located near the core and are exposed to much higher neutron fluence than RPV

# Russian Regulatory Guides for Irradiation Embrittlement

The Regulatory Guide the following dependence must be used for calculating the irradiation embrittlement of VVER-440 vessel materials with low nickel content at the irradiation temperature of 270°C:

$$\Delta T, \text{ }^{\circ}\text{C} = A_F F^{1/3}$$

where  $A_F=18$  for the base metal,

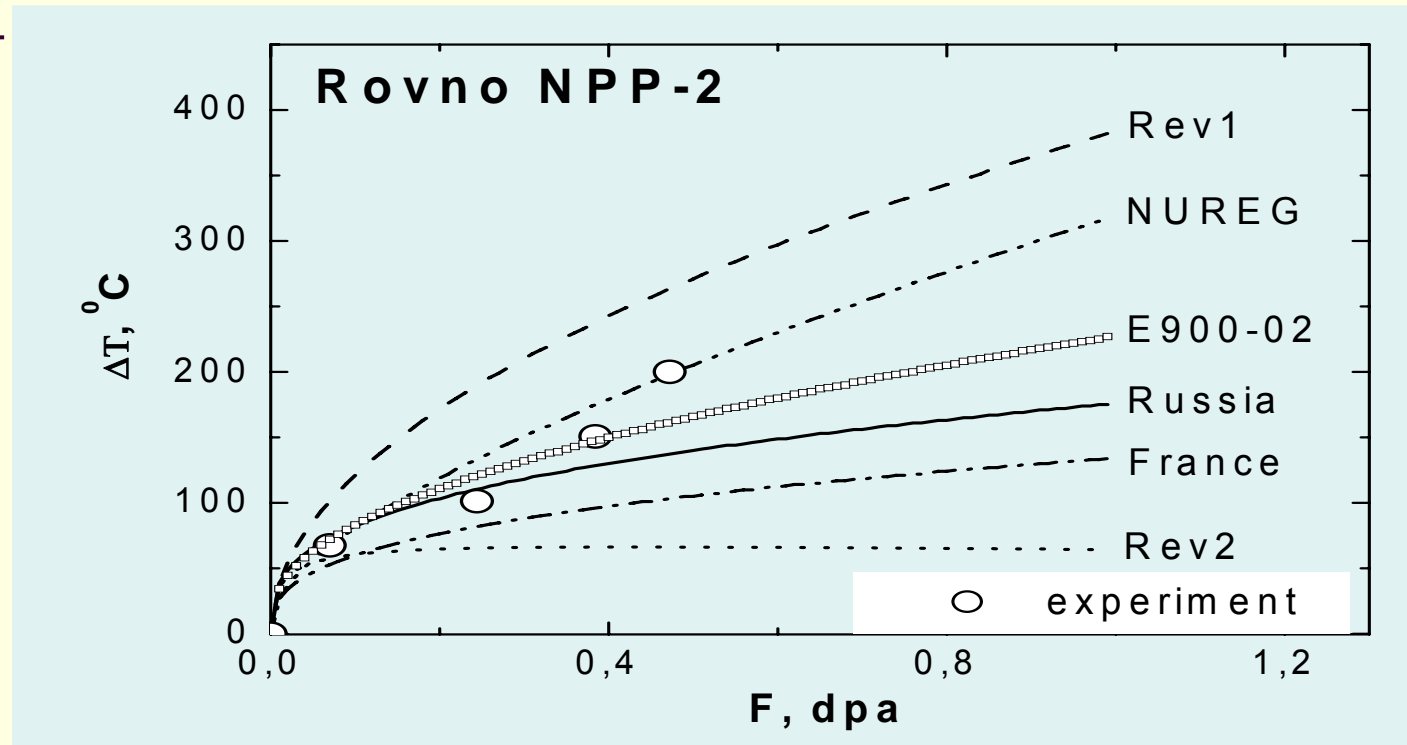
$A_F = 800 (C_P+0.07 C_{Cu})$  for welds,

$F$  is the fast neutron fluence in units of  $10^{18}$  n/cm<sup>2</sup> (E>0.5 MeV),

$C_P$  и  $C_{Cu}$  are the phosphorus and copper contents (wt.%),  
respectively

**However, recent data on irradiation embrittlement of surveillance specimens in VVER-440 units of several nuclear power plants deviate essentially from the normative dependence at fast neutron fluences  $F$  higher than  $2 \times 10^{20}$  n/cm<sup>2</sup> and reveal a significant enhancement of embrittlement at these fluences**

# Comparison of Experimental Data with Regulatory and Standard Guides



*Comparison of experimental data from Rovno NPP-2 with Regulatory and Standard Guides available: Russian (Russia), French (France), and American ones (NRC Regulatory Guide 1.99, Revision 1, 1977 (Rev 1), NRC Regulatory Guide 1.99, Revision 2, 1988 (Rev 2), NUREG/CR-6551, 1998 (NUREG), E900-02, 2002 (E900-02))*

# A Model of Embrittlement at High Neutron Fluences

---

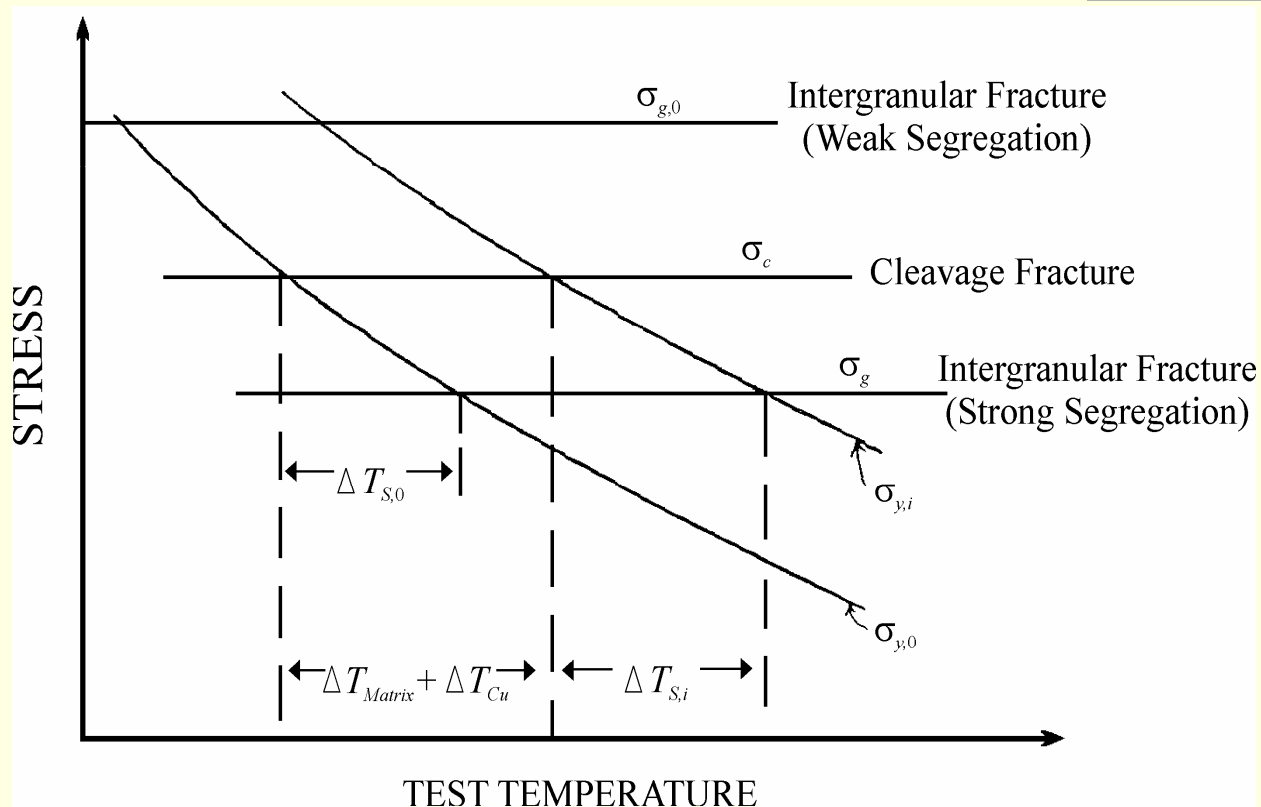
The proposed model accounts for the mechanisms of matrix hardening and intergranular fracture.

Matrix hardening leads to yield strength  $\sigma_y$  increase accompanied with the DBBT shift  $\Delta T_1$ .

The second mechanism linked to the phosphorus segregation and leads to the decrease of intergranular fracture stress  $\sigma_F$  and to corresponding DBBT shift  $\Delta T_2$ . If both mechanisms operate, then the total DBTT shift is

$$\Delta T = \Delta T_1 + \Delta T_2$$

# A Model of Embrittlement at High Neutron Fluences



Schematic Diagram of Intergranular Fracture Criterion  
(Bolton et al, 1996)

# A Model of Embrittlement at High Neutron Fluences

**Beginning with some critical dose  $F_c$ ,  $\sigma_y$  exceeds  $\sigma_F$  and the crack propagation in dynamic Charpy tests may occur predominantly on grain boundaries:**

$$\Delta T = A_F F^{1/3} + n A_F (C_P^g(F) - C_P^g(F_c))$$

**where  $n=0$  at  $F < F_c$  and  $n=1$  at  $F \geq F_c$ ,  $F_c$  and  $A_F$  are fitting parameters, the function  $C_P^g$  is obtained by modeling of phosphorus accumulation on GB**

# GB model in multicomponent alloys

- By analogy with an approach by Guttman (1975) and Defai and Prigogine (1951):

GB is a flat layer of the width  $d$  with chemical potentials of components  $\mu_k^g$  and thermal equilibrium point defect concentrations  $C_{\alpha e}^g$  different from those in the matrix,  $\mu_k^b$  and  $C_{\alpha e}^b$ . GB is a perfect sink of PD separated from the matrix by a distance  $b$ .

- Component and PD fluxes  $J_k$  and  $J_\alpha$  ( $\alpha=i,v$ ) in the matrix are proportional to gradients of chemical potentials.

- Component and PD fluxes  $j_k$  and  $j_\alpha$  from the matrix to GB are proportional to differences of chemical potentials in the matrix and on GB

# Combined radiation-induced and thermal equilibrium segregation at GB

- Under the steady-state

$$J_k = j_k = 0, \quad j_v = j_{v0} = j_i = j_{i0} = \varepsilon KR_g$$

where  $\varepsilon$  is the cascade efficiency,  $K$  is the PD generation rate, index "0" denotes an alloy with no segregation,  $R_g$  is the size of a region from which PD are absorbed on GB (of the order of PD free path length)

Solving the equation for  $j_k$  in steady-state conditions one can obtain:

$$\mu_k^g = \mu_k^b + \left( \frac{d_{ki}^b C_i^b}{D_k^b} \mu_i^b - \frac{d_{kv}^g C_v^b C_k^g}{D_k^b C_k^b} \mu_v^b \right)$$

where "g" and "b" indexes denote GB and its nearest plane in the matrix

*The "kinetic" term in brackets disturbs a "thermodynamic" equilibrium between component concentrations on GB and in the matrix*

# Combined radiation-induced and thermal equilibrium segregation at GB

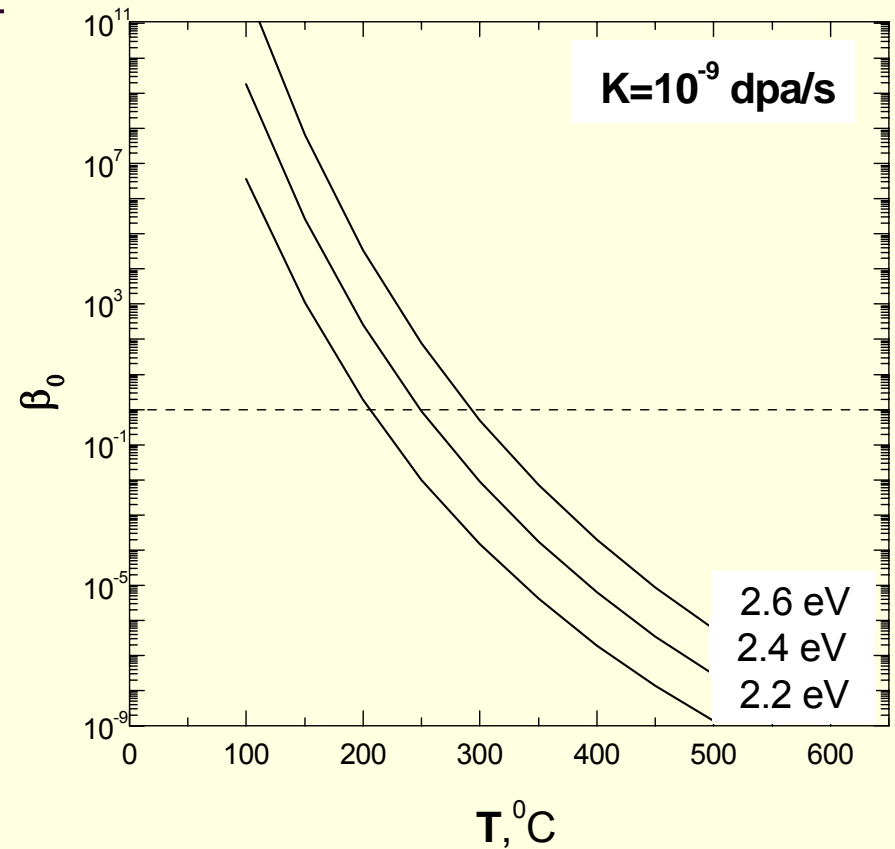
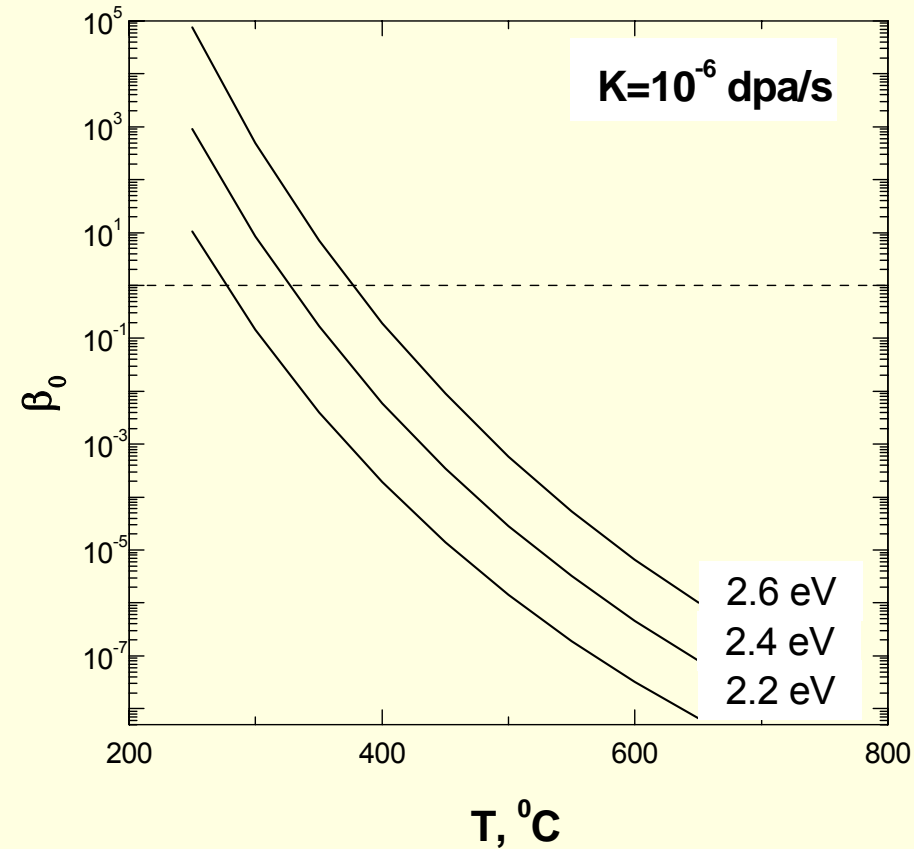
Approximate analytical solution of for  $C_k^g$  can be obtained in two limiting cases:  $\beta_0 \ll 1$  and  $\beta_0 \gg 1$

$$\beta_0 = \frac{\varepsilon K b R_g}{D_{Ns}^b \cdot C_{ve}^g / C_{ve}^b}$$

where  $D_{Ns}^b$  is the self-diffusion coefficient of component "N" near GB.

Physically,  $\beta_0$  equals the ratio of the PD flux from the region Rg to GB due to irradiation and the flux of thermal vacancies between GB and the matrix

# Combined radiation-induced and thermal equilibrium segregation at GB



The dependence of  $\beta_0$  on temperature and on effective activation energy of self-diffusion  $E_s = E_{sd} - (E_v^{f,b} - E_v^{f,g})$  at dose rates of  $10^{-6}$  dpa/s and  $10^{-9}$  dpa/s

# Combined radiation-induced and thermal equilibrium segregation at GB

At relatively high temperatures  $\beta_0 \ll 1$ . Then a “thermodynamic” equilibrium is established. In this case

$$C_k^g = \frac{C_{k0} \left( C_{v0}^b / C_{v0}(\infty) \right)^{g_{kN}^0} \cdot \exp(\Delta G_{kN} / kT)}{\sum_j^n C_{j0} \left( C_{v0}^b / C_{v0}(\infty) \right)^{g_{jN}^0} \cdot \exp(\Delta G_{jN} / kT)}$$

Where  $C_{v0}^b = C_{v0}(b)$        $g_{kN}^0 \sim d_{kv} d_{Ni} - d_{ki} d_{Nv}$

The difference  $\Delta G_{kN}$  in free enthalpies of "k" and "N" components on GB was defined by Guttmann (1975).

*This relation allows to treat the competition and cooperation of components both in the equilibrium adsorption on GB and in RIS near GB*

# Combined radiation-induced and thermal equilibrium segregation at GB

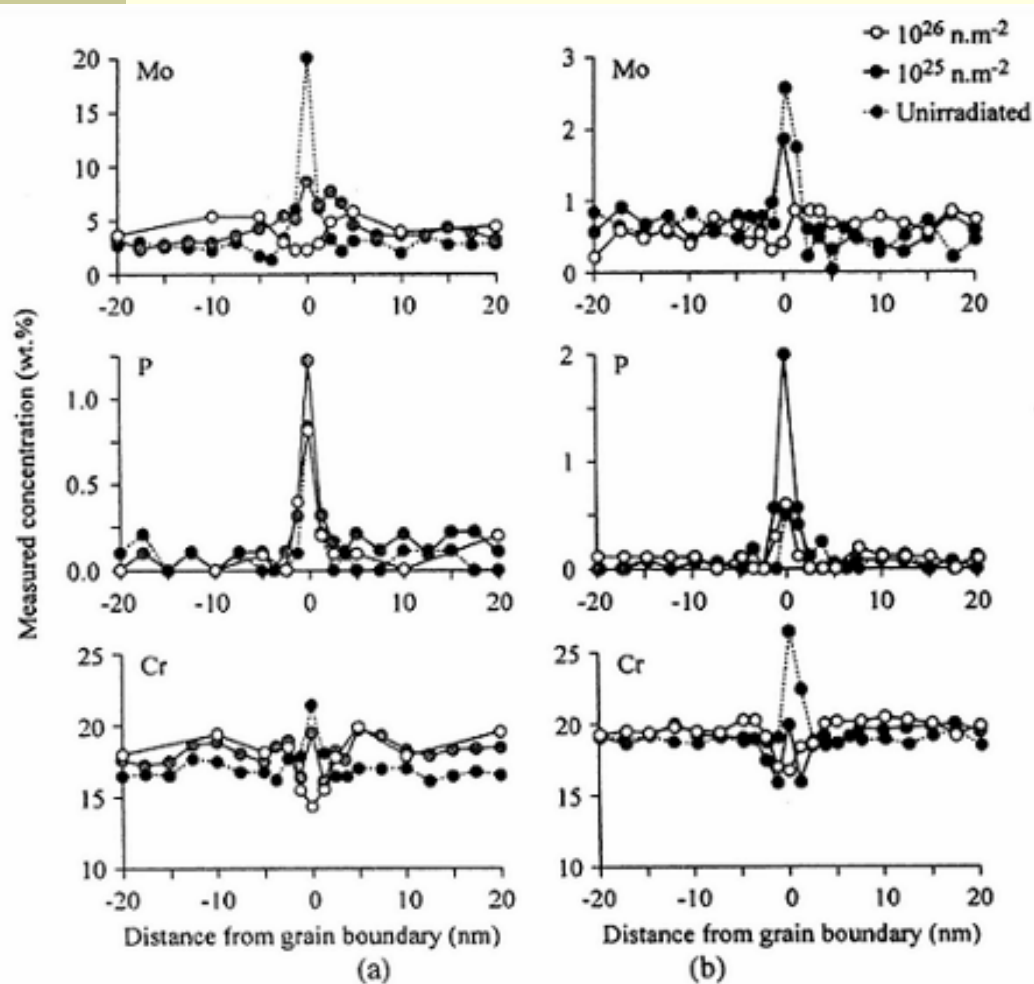
At relatively low temperatures where  $\beta_0 \gg 1$ , a “kinetic” equilibrium is established due to PD fluxes to GB. In this case

$$C_k^g = \frac{C_k^b \exp(\Delta G_{kN} / kT) d_{ki}^b / d_{kv}^b}{\sum_j C_j^b \exp(\Delta G_{jN} / kT) d_{ji}^b / d_{jv}^b}$$

Where  $C_k^b$  is defined by RIS

# Fe-Cr-Ni alloys and austenitic steels

*Typical FEGSTEM-EDXS grain boundary composition profiles for molybdenum, phosphorus and chromium after various treatments in: (a) type-316; (b) type-304, irradiated in BWR at 288 °C (Goodwin et al., 2000)*



Two possible mechanisms of Cr “presegregation” on GB: (1) Gibbsian adsorption and (2) nonequilibrium thermal segregation.

Simonen, Bruemmer, 1997;  
Bruemmer, 1999: Cr enrichment cannot be explained by simple solute-vacancy interaction because too large Cr-vacancy binding energies are required

# Temper embrittlement

In the absence of irradiation reveals (Guttmann's relations)

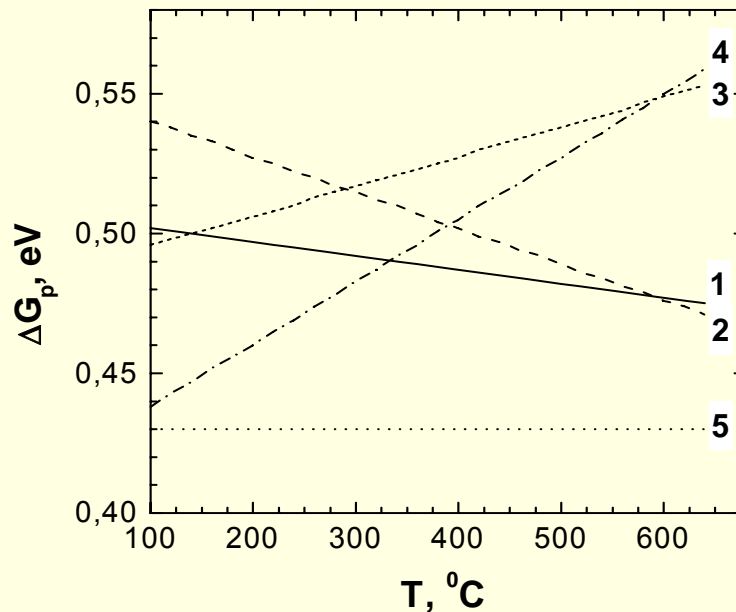
and only gibbsian adsorption (GA)

$$\mu_k^b = \mu_k^g$$

$$C_k^g = \frac{c_k^b \exp(\Delta G_{kN} / kT)}{\sum_j^n c_j^b \exp(\frac{\Delta G_{jN}}{kT})}$$

Accumulation of P and S on GB leads to intergranular embrittlement at enhanced temperatures (400-500 °C) called “temper embrittlement”

GA is the driving force for it



# Kinetics of Phosphorus Accumulation at GB

McLean's diffusion model defines the rate of P accumulation

After the quick decreasing the temperature from  $T_1$  to  $T_2$

$$D_{ks} \frac{\partial^2 C_k}{\partial x^2} = \frac{\partial C_k}{\partial t}$$

$$C_k^g(t) = C_k^{gs} - C_{k0}(\alpha_2 - \alpha_1) \exp\left(\frac{4D_{ks}t}{\alpha_2^2 d^2}\right) \operatorname{erfc}\left(\frac{2\sqrt{D_{ks}t}}{\alpha_2 d}\right)$$

$$C_k^{gs}(T_1)/C_{k0} = \alpha_1$$

$$C_k^{gs}(T_2)/C_{k0} = \alpha_2$$

# Kinetics of Phosphorus Accumulation at GB under irradiation

For modeling of phosphorus accumulation at GB a modification of the McLean's model of temper embrittlement was performed (Pechenkin et al., 2001)

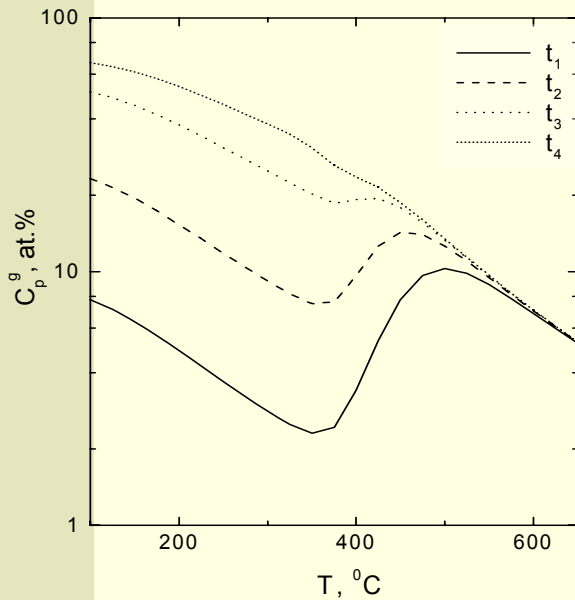
The modification accounts for radiation-enhanced diffusion of P in the matrix via vacancy and interstitial mechanisms, radiation-induced segregation of P near GB and Gibbsian adsorption on GB

Two essentially different sets of diffusion parameters (Set 1 and Set 2) were used. The major difference of the sets concerns the vacancy migration energy (0.6 eV in Set 1 and 1.2 eV in Set 2, respectively), the interstitial migration energy (0.3 eV in Set 1 and 0.15 eV in Set 2, respectively), the energy of binding between P atom and an interstitial (0.3 eV and 0.15 eV, respectively)

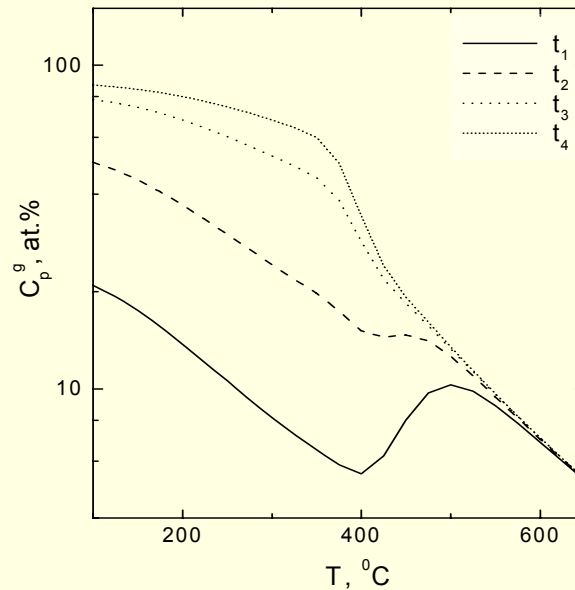
Point defect generation rate  $K = 2.8 \times 10^{-9}$  dpa/s for locations of surveillance specimens and  $K = 3 \times 10^{-10}$  dpa/s for inner vessel surfaces

# GB Phosphorus Accumulation in the VVER-440 RPV Steel

a)



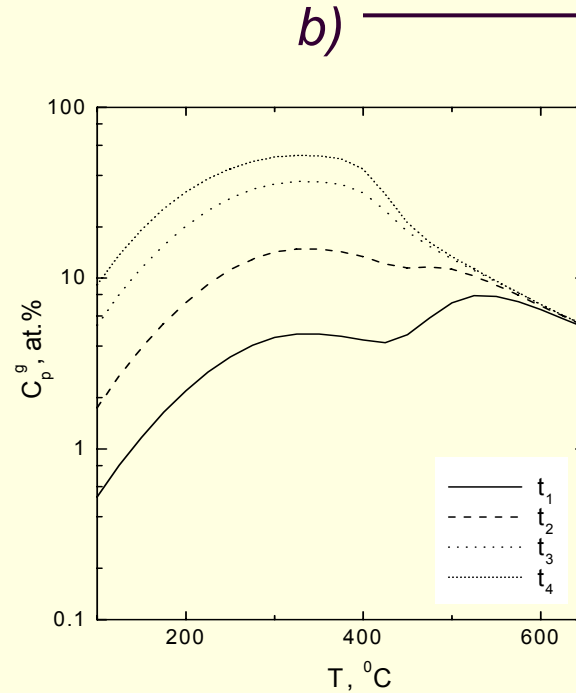
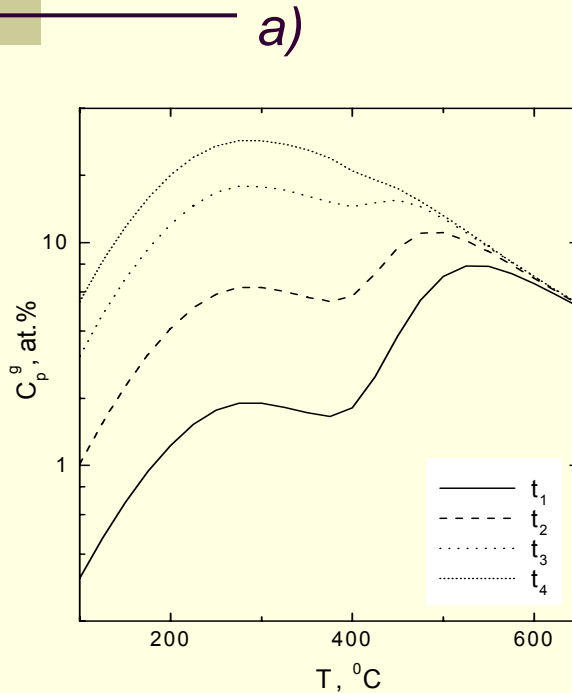
b)



Set 1 of parameters for four exposures: one month ( $t_1$ ), one year ( $t_2$ ), 10 years ( $t_3$ ) and 30 years ( $t_4$ ):  
a) inner vessel surface  
b) surveillance specimens

The calculations were carried out for phosphorus content of 0.012 wt. % and point defect sink strength of  $\rho_s = 10^{14} \text{ m}^{-2}$  corresponding to a typical dislocation density in a neutron irradiated RPV steel

# GB Phosphorus Accumulation in VVER-440 RPV Steel



Set 2 of parameters for four exposures: one month ( $t_1$ ), one year ( $t_2$ ), 10 years ( $t_3$ ) and 30 years ( $t_4$ ):

a) inner vessel surface

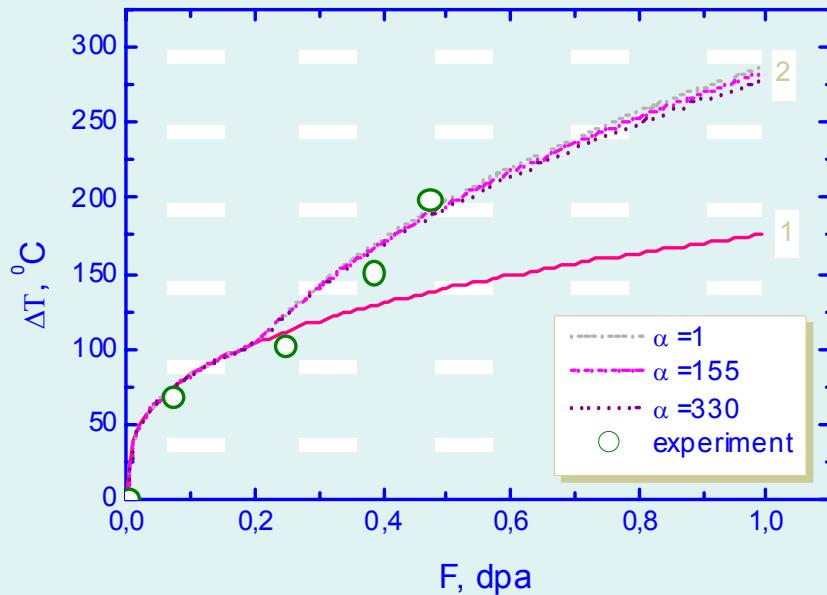
b) surveillance specimens

# Kinetics of Phosphorus Accumulation at GB

The difference in phosphorus accumulation at low temperatures is related to the difference in mechanisms governing average PD concentrations in the bulk. These concentrations are determined by the PD sink strength for the Set 1 of parameters and by the PD recombination for the Set 2. One can obtain the following estimates of radiation enhanced phosphorus diffusion coefficients  $D_{P1}$  for Set 1 and  $D_{P2}$  for Set 2:

$$D_{P1} \cong \frac{\varepsilon K}{\rho_s} \exp\left(\frac{E_b}{kT}\right), \quad D_{P2} \cong \sqrt{\frac{\varepsilon K D_0}{\mu_R}} \exp\left(\frac{2E_b - E_v^m}{2kT}\right)$$

# Embrittlement in VVER-440 RPV at High Neutron Fluences



*Curve 2 - the proposed model*

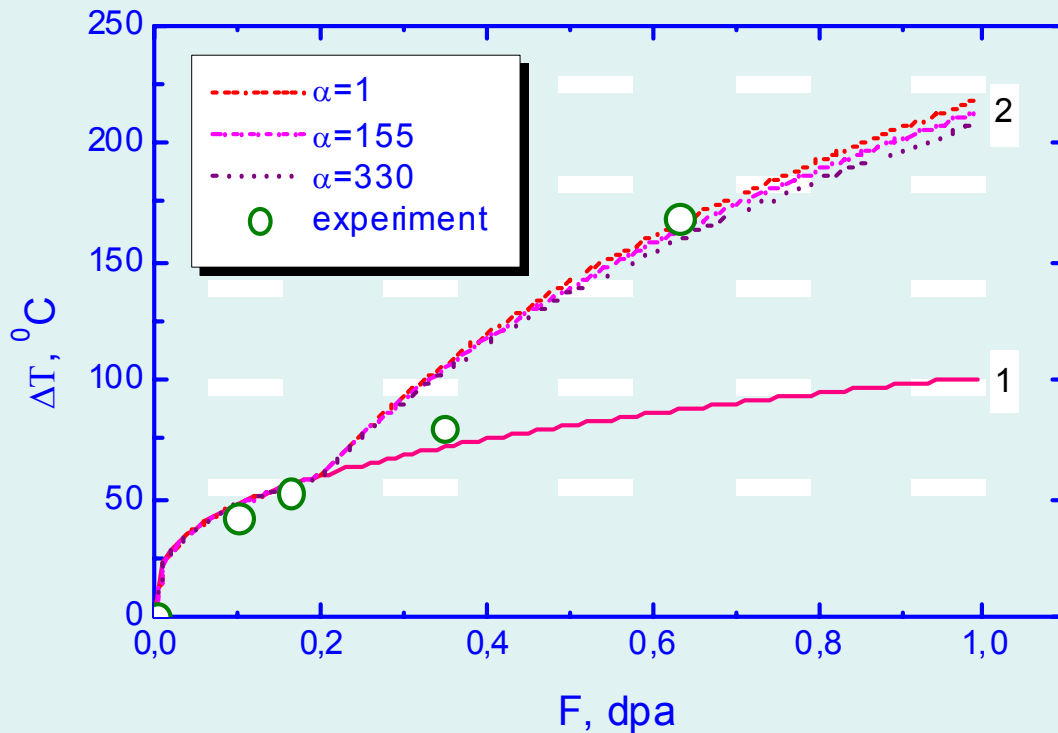
*Curve 1 - the normative dependence*

*Open circles – experimental data for surveillance specimens of VVER-440 vessel base metal in Rovno NPP-2 (0.012 P, 0.11 Cu, 0.28 Ni, wt. %)*

*The dose is given in dpa calculated from the relation 0.1 dpa per  $10^{20}$  n/cm<sup>2</sup> ( $E > 0.5$  MeV)*

The coefficient  $\alpha$  is equal to the ratio of phosphorus concentration on GB before the start of irradiation and its content in the matrix. It takes into account a possible adsorption of phosphorus on GB during manufacturing the vessel

# Embrittlement in VVER-440 RPV at High Neutron Fluences



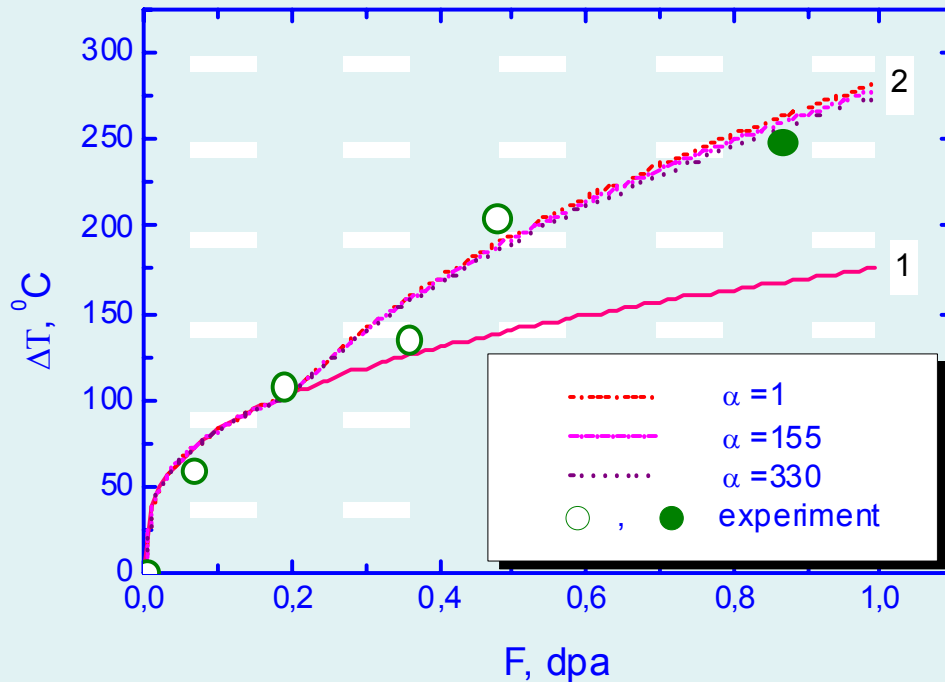
*Curve 2 - the proposed model*

*Curve 1 - the normative dependence*

*Open circles – experimental data for surveillance specimens of VVER-440 vessel base metal in Armenian NPP-2 (0.013 P, 0.13 Cu, 0.19 Ni, wt. %)*

*$A_F = 14$  for this NPP (Shtrombach, 1998)*

# Embrittlement in VVER-440 RPV at High Neutron Fluences



*Curve 2 - the proposed model*

*Curve 1 - the normative dependence*

*Circles – experimental data for surveillance specimens of VVER-440 vessel base metal in Kolskaya NPP-2 (0.011 P, 0.09 Cu, 0.15 Ni, wt. %)*

The DBTT shift in specimens irradiated with the highest neutron fluence of  $8.3 \times 10^{20}$  n/cm<sup>2</sup> ( $E > 0.5$  MeV) has been measured after the model prediction (filled circle)

# Conclusions

- ❑ Irradiation causes a complex of structural changes in RPV: formation of radiation defects, phase changes with the occurrence of ultrafine precipitates, intragranular and intergranular impurity segregation
- ❑ At early stages the radiation-induced precipitates dominate. The radiation defects (dislocation loops) dominate at later stages of irradiation
- ❑ At enhanced neutron fluences the contribution of intergranular embrittlement induced by the phosphorus segregation on grain boundaries is important